ELSEVIER

Journal of Atmospheric and Solar-Terrestrial Physics 70 (2008) 621–626

Journal of ATMOSPHERIC AND SOLAR-TERRESTRIAL PHYSICS

www.elsevier.com/locate/jastp

The numerical MHD simulation of solar flares

A.I. Podgorny[a,*], I.M. Podgorny[b], N.S. Meshalkina[c]

[a]Lebedev Physical Institute RAS, Leninsky Prospect, 53, Moscow 119991, Russia
[b]Institute for Astronomy RAS, Pyatnitskaya Street, 48, Moscow 119017, Russia
[c]Institute for Solar-Terrestrial Physics SO RAS, Lermontov Street, 126a, Irkutsk 664033, Russia

Accepted 27 August 2007
Available online 5 October 2007

Abstract

The 3D MHD calculations carried out above the active region AR 0365 before the flare on May 27, 2003 show solar flare energy accumulation with current sheet (CS) creation in the singular line (SL) vicinity. The maximal radio-emission intensity measured with the SSRT radio telescope (Irkutsk) coincides with the current density maximum in CS. The obtained results confirm the solar flare electrodynamical model and open the possibility for improving the solar flare prognosis.

Keywords: Solar flare; Current sheet; Radio-emission; MHD

1. Introduction

The flare electrodynamical model (Fig. 1) is based on the numerical 3D MHD simulation of energy accumulation in the current sheet (CS) magnetic field (Podgorny and Podgorny, 1992, 2001, 2006). The model explains phenomena observed during a flare including visible ribbons, X-ray radiation, coronal mass ejection, and spectra of solar flare cosmic rays (Podgorny and Podgorny, 2006).

It has been shown in the MHD numerical experiments that CS forms (Podgorny and Podgorny, 1992) before the onset of the flare in the corona in the magnetic singular line (SL) vicinity as a result of focusing of disturbances coming from the photosphere—in particular, new magnetic flux, whose direction is opposite to that of the old flux of the active region emerges (Podgorny and Podgorny, 2001). CS is stable for a long period, and energy is stored in its magnetic field, then it rapidly realized during the solar flare when CS transforms into an unstable state. CS is highly stable during its formation due to the presence of a normal magnetic field component in CS and the plasma flow along the sheet. This stage is followed by quasi-stationary evolution of CS, during which the total mass of the plasma in CS decreases due to the ejection of plasma accelerated by the magnetic tension from CS. The plasma density is reduced, so that the plasma density remains virtually constant at the center of CS and decreases near its boundary.

The basic dissipation mechanism during the explosive decay is reconnection, which results in plasma heating in the vicinity of SL. Depending on the initial condition of the field in the active region

*Corresponding author. Tel.: +7 495 408 6219; fax: +7 495 408 6102.
E-mail address: podgorny@fian.fiandns.mipt.ru (A.I. Podgorny).

1364-6826/$ - see front matter
doi:10.1016/j.jastp.2007.08.043

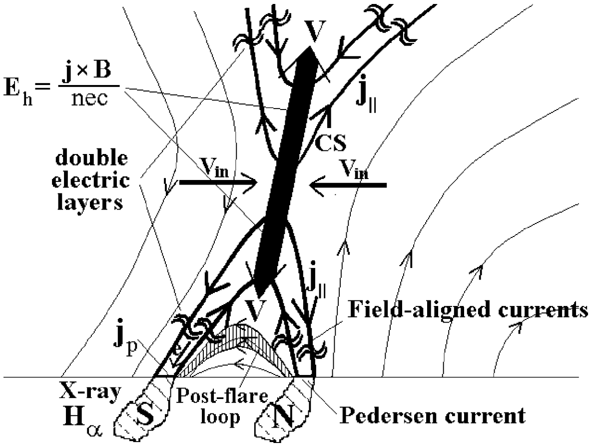

Fig. 1. The flare electrodynamical model. Thin lines and thin arrows show magnetic field line. Thick lines and thick arrows show field-aligned current generated by the Hall electric field.

and the character of photospheric disturbances in the preflare state, CS can be inclined to the solar surface at various angles. The solar flare model for the vertical CS is shown in Fig. 1. In that case the solar flare and CME develop simultaneously in the same explosive event. The plasma flows into CS from both sides with the velocity V_{in} together with frozen-in magnetic field lines spreading along the CS upward and downward during field line reconnection. The $\mathbf{j}\times\mathbf{B}/c$ force accelerates the plasma, and the upward plasma stream ejects the solar material into space—coronal mass ejection develops. The plasma accelerated downward, with shrinking magnetic lines, forms a postflare loop.

An important property of CS is the Hall electric field $\mathbf{E}_h = \mathbf{j}\times\mathbf{B}/nec$ generation inside the sheet, whose direction coincides with the plasma velocity along CS. Since the plasma conductivity in the magnetic field is highly anisotropic, the Hall electric field generates electric currents along the magnetic lines intersecting CS. The field-aligned currents are shown by bold lines in Fig. 1. These field-aligned currents are closed inside the photosphere due to the presence of neutral atoms there. The electrons accelerated in the upward field-aligned current precipitate onto the chromosphere, giving rise to the glow of flare ribbons and hard X-ray emission. Typically, the energies can reach several hundred keV. The electrons heat the chromosphere and produce chromosphere evaporation filling the loop by plasma.

The primary flare energy release in the corona has been confirmed by measurements of hard X-ray emission (Tsuneta et al., 1997; Lin et al., 2003). The coronal X-ray source with the temperature of $\sim$3 keV has been observed in RHESSI (Lin et al., 2003) measurements above the arch. The photospheric X-ray sources produced by electron beams with energy up to $\sim$100 keV are located in the magnetic arch footpoints. Apparently, these electrons gain their energy accelerating along field-aligned currents.

Several models of CME and solar flares creation are based on twisted flux rope ejection (Lin, 2004; Forbes, 1991; Mikic et al., 1988; Amari et al., 2000; Roussev et al., 2004; Kliem et al., 2004). The plasma acceleration can be described as rope current interaction with the image current situated under the photosphere. If the rope current $\mathbf{I}$ is directed perpendicular to the arch magnetic field $\mathbf{B}_{\mathrm{ar}}$ of an active region, the force $\mathbf{I}\times\mathbf{B}_{\mathrm{ar}}/c$ also appears that can supply additional acceleration or deceleration of the rope. In the point, where these forces are equal and oppositely directed (upward and downward), the unstable equilibrium takes place. Such a situation is considered by Lin (2004), Forbes (1991), and Mikic et al. (1988). The rope accelerated upward stretches magnetic field into configuration of CS, where magnetic energy is effectively accumulated for a solar flare, and the ejected rope produces CME.

The most difficult problem of such models is the explanation, how such a rope can be created. In the works of Lin (2004) and Mikic et al. (1988) it is supposed, that the rope exists from the very beginning. Amari et al. (2000) and Roussev et al. (2004) attempt to obtain the rope creation in the corona by twisting of foot-points of the arches and by shear-type foot-point motion on the photosphere. In the unstable equilibrium a rope should be created in very short time before the ejection. The rope appearance can be also explained by its emergency from-under the photosphere. Such an emergence has to create tremendous photospheric disturbances before the flare. The interesting mechanism of flare and CME is proposed by Kliem et al. (2004). The rope becomes unstable due to the kink instability at critical magnetic lines twisting, and, as a result, rope is ejected.

The interesting results have been obtained by simulations of CS creation in the corona for different field approximations (Forbes and Priest, 1984; Rickard and Priest, 1994; Podgorny and Podgorny, 1998; Archontis et al., 2006). The CS creation and energy storage in the CS magnetic field before a flare has been demonstrated in 3D MHD numerical simulation (Bilenko et al., 2002). For these purposes the active region magnetic field is approximated by the field of magnetic dipoles placed under the photosphere. This approximation permits to show the energy accumulation of 10^{33} erg before the Bastille flare. But such an approximation does not include all peculiarities of the photospheric preflare magnetic field, and CS location cannot be obtained with high degree of precision. To improve precision a method of setting the observed photospheric magnetic field as a boundary condition is developed. Here we present the result of simulation of CS creation in the real active region that appears due to the real photospheric disturbances observed before a flare. In this simulation no assumptions about the flare mechanism are done.

2. Numerical simulation

The AR 0365 has been chosen for simulation since its magnetic field is not very complicated. The observed change of the photospheric magnetic field leads to evolution of the coronal magnetic configuration (Podgorny and Podgorny, 2006). The temporal system of resistive 3D MHD equations for compressible plasma is solved in the computational domain ($0<x<1$, $0<y<0.5$, $0<z<1$ in dimensionless units). $L_0 = 1.2\times10^{10}$ cm is used as the length unit. Y axis is directed from the Sun. X is directed to the west, and Z is directed to the south. The photospheric boundary ($y=0$, $0<x<1$, $0<z<1$) of numerical domain contains the active region AR 0365. The observed line-of-sight magnetic field component distribution on the photosphere ($y=0$, $0<x<1$, $0<z<1$) obtained by SOHO MDI is used for setting initial and boundary conditions.

The initial magnetic field in the computational domain is set three days before the flare on May 27, 2003, because observations (Ishkov, 2001) show that the photospheric magnetic field begins to change in 1–2 days before the flare. The potential field is taken for setting the initial condition, because three days before a flare there are no essential disturbances in the corona, and so the currents can be neglected. The potential field is calculated in the computational domain by solving numerically the Laplace equation using a finite-difference scheme on the same grid as for MHD equations. An inclined derivative is employed as a boundary condition on the photosphere boundary, since the line-of-sight field component is generally inclined at some angle to the photosphere. The field on the nonphotospheric boundary is small and does not influence the solution of the Laplace equation that is verified by solving with different types of conditions on the nonphotospheric boundary.

For setting boundary conditions, it is necessary to use magnetic vector evolution on the photosphere. However, SOHO MDI magnetic maps give data only for the magnetic component directed along the line-of-sight. Magnetic components parallel to the photosphere are taken from distribution of the potential magnetic field, that is calculated also by numerical solving of the Laplace equation. Such an approximation is possible, because CS is located high in the corona, so the CS magnetic field does not influence the photospheric magnetic field strongly.

In the chosen corona region with the height $\sim 0.1\ R_{\odot}$, the plasma density and the temperature do not strongly change in space. So the initial plasma density and the temperature are set to be constant in space. Their values are corresponded to conditions in the low corona $\rho_0 = 10^8\,\mathrm{cm}^{-3}$ and $T_0 = 10^6$ K. The initial velocity is taken to be zero.

The process of CS creation takes place sufficiently high, $\sim 1/20\ R_{\odot}$, and the plasma density change on the photospheric boundary at $\beta \ll 1$ hardly influence CS creation. The plasma density ρ on the photosphere is set to be constant, equal to $\rho_0 = 10^8\,\mathrm{cm}^{-3}$. The normal to the photosphere derivative of the temperature is set to be zero ($\partial T/\partial n = 0$). The condition for the plasma velocity on the photosphere is $\partial \mathbf{V}/\partial n = 0$. It is assumed that the currents on the nonphotospheric boundary may be neglected. Therefore, $\mathbf{B}$ components parallel to the nonphotospheric boundary are set from $\mathrm{rot}\,\mathbf{B} = 0$ condition. The normal $\mathbf{B}$ component is set from $\mathrm{div}\,\mathbf{B} = 0$ that is found automatically from solution of MHD equations, if a difference scheme conservative relative to magnetic flux is used. The free-exit conditions on the nonphotospheric boundary are approximated as $\partial\rho/\partial n = 0$, $\partial T/\partial n = 0$, $\partial \mathbf{V}/\partial n = 0$.

The system of 3D MHD equations is solved numerically by an absolutely implicit scheme (Podgorny and Podgorny, 2004). The scheme is conservative relative to the magnetic flux. It means that instead of a magnetic field vector, the averaged magnetic fluxes per unit of square through boundaries of grid cells are used. The total flux through each cell boundary remains the same at passing to

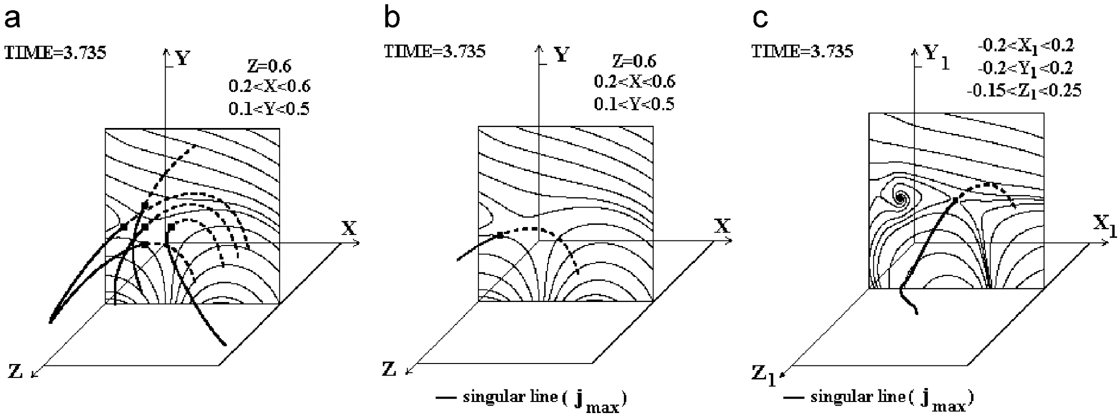

Fig. 2. (a) Magnetic line projections on the $z = 0.6$ plane and magnetic lines in 3D space (thick lines, dashed lines are located behind the $z = 0.6$ plane); (b) the singular line that intersects the plane $z = 0.6$; (c) the singular line (thick line), here axis Z_1 is parallel to the singular line, axes X_1 and Y_1 are perpendicular to the singular line in the point ($x = 0.25$, $y = 0.25$, $z = 0.6$).

the next time step. It means, that the finite-difference analog of $\mathrm{div}\,\mathbf{B}$ is equal to zero, if $[\mathrm{div}\,\mathbf{B}] = 0$ for the initial field. This scheme has been realized in the PERESVET code. The calculations are carried out with a grid $101 \times 51 \times 101$.

The finite-difference analog of $\mathrm{div}\,\mathbf{B}$ for the initial potential field calculated by solving numerically of the Laplace equation is equal to zero with precision of 0.5×10^{-3} in dimensionless units. This precision of $[\mathrm{div}\,\mathbf{B}] = 0$ is preserved during entire time of calculations. The equality of $[\mathrm{div}\,\mathbf{B}] = 0$ is controlled at each time step.

The 3D numerical MHD simulation (Podgorny and Podgorny, 1992, 2001) has shown that CS appears in SL vicinity due to magnetic disturbances focusing. The current density in CS increases with time. The current density maximum is situated on SL. The current is directed along this line. SL has been found as a line passing through the position of the current density maximum. The coronal magnetic field configuration above AR 0365 contains several SL. However, the calculations show that CS appearing in the vicinity of SL that intersects the plane $z = 0.6$ on the interval $0.2 < x < 0.5$ is the most powerful. Here, we restrict ourselves only to analyze this SL and compare calculation results with the biggest radio-emission flare burst observed on the SSRT radio telescope.

The analysis of magnetic field behavior in planes perpendicular to the photosphere shows that the best conformity of a magnetic configuration to the CS magnetic field is revealed in the plane $z = 0.6$. The magnetic field configuration before the flare is shown in Figs. 2a and b. Here, the magnetic lines located behind the $z = 0.6$ plane are indicated by dashed lines. The zero X-point in the plane perpendicular to SL must coincide with the point of SL intersection of this plane. However, the zero X-point in the $z = \mathrm{const}$ plane does not coincide with the point of SL intersection of this plane (Fig. 2(b)), because SL is not normal to this plane. It means that the current density maximum in the $z = \mathrm{const}$ plane does not coincide exactly with the magnetic X-point. Such an exact coincidence takes place in X_1Y_1 plane (Fig. 2(c)). Here Z_1 axis is tangential to SL in the point of the plane intersection; X_1 and Y_1 axes are perpendicular to this line. Coincidence of the current maximum and the magnetic X-point in this plane proves correctness of calculations. It is reasonable to conclude that the maximum of plasma heating must occur in this point during a flare, because here the current density maximum is situated in this place.

The computational domain moves with an active region on the solar disk due to Sun rotation. The calculations show that only a negligible shift of the current density maximum inside the computational domain occurs in the time interval starting 12 h before the flare. This fact permits to obtain the maximum current density coordinates at any time within this interval in spite of the different time scales in calculations and in the reality.

3. Flare radio emission

The May 27, 2003 flare at 02:53:28.54 has produced the strong increase of the brightness temperature observed by the SSRT radio telescope

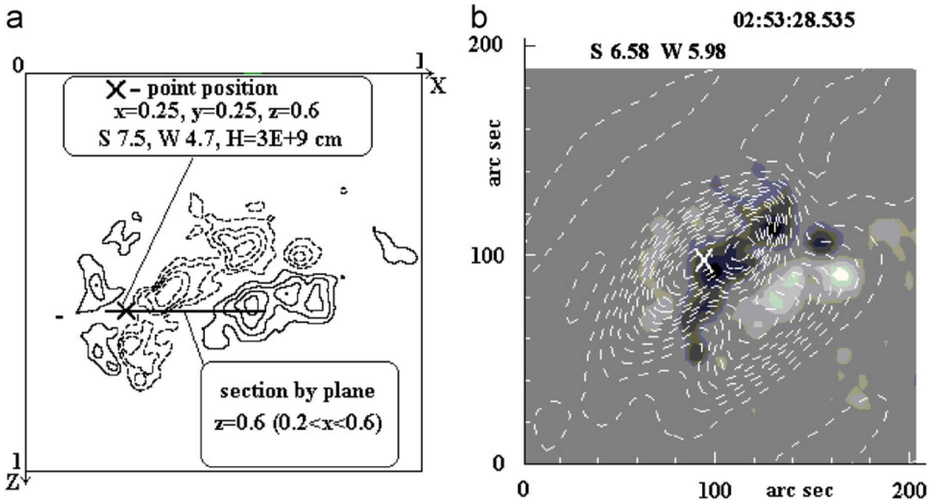

Fig. 3. (a) Lines of equal normal component of the photospheric magnetic field (dashed lines show negative field), the cross shows the current density maximum; (b) lines of equal intensity of radio emission and the flare magnetogram, the cross shows the brightness temperature maximum.

at the 5.2 cm wave. This wave belongs to the high frequency continuum appearing simultaneously with the flare X-ray emission (Benz et al., 2005). The observed maximum of the brightness temperature was 1.24×10^7 K. Distribution of the radio emission intensity of the flare on May 27, 2003 at 02:53:28.54 in the AR 0365 is presented in Fig. 3(b) in the figure plane (perpendicular to the line-of-sight). The magnetogram of the magnetic field component along the line-of-sight is also shown. The SOHO MDI magnetogram (http://soi.stanford.edu/magnetic/index5.html) is used. Heliocentric coordinates of the brightness temperature maximum are S6.58 W5.97. This maximum is indicated by the cross in Fig. 3(b).

Coordinates of singular point in the computational domain are ($x = 0.25$, $y = 0.25$, $z = 0.6$). Its heliocentric coordinates on May 27, 2003 at 02:53:28.54 are S7.541 W4.692. B (normal) = const lines calculated in potential approximation on the photosphere are shown in Fig. 3(a). Lines of equal intensity of the radio emission and the flare magnetogram are shown in Fig. 3(b) for comparison. The position of the flare is marked by a cross in both figures. The cross in Fig. 3(a) is a projection of the point ($x = 0.25$, $y = 0.25$, $z = 0.6$) on the photosphere along the normal, and the cross in Fig. 3(b) is the position of the radio emission maximum. Positions of the both maxima coincide with accuracy about 1°. This coincidence is in agreement with the electrodynamical solar flare model. The inexactitude does not surpass the accuracy of setting boundary conditions from the photospheric magnetic field, the accuracy of calculation, and accuracy of obtaining coordinates on the solar disk.

4. Conclusion

The comparison of the results of numerical MHD simulations and radio emission observations demonstrates a convincing evidence of correctness of the electrodynamical solar flare model based on energy accumulation in the magnetic field of CS appeared above an active region. These results demonstrate that MHD simulations permit tracing the flare position from analyzing preflare photospheric magnetic maps.

Acknowledgements

Authors acknowledge fruitful cooperation with A.T. Altyntsev, V.V. Grechnev, and A.I. Hlystova. The work was supported by Russian projects of RFBR Nos. 06-02-16006, 05-07-90147, 04-02-39003.

References

Amari, T., Luciami, J.F., Mikic, Z., Linker, J.J., 2000. Astrophysical Journal 529, L49.

Archontis, V., Galsgaard, K., Moreno-Insertis, F., Hood, A.W., 2006. Astrophysical Journal 645, L161.

Benz, A., Grigis, P.C., Csillaghy, A., Saint-Hilaire, P., 2005. Solar Physics 226, 122.

Bilenko, I.A., Podgorny, A.I., Podgorny, I.M., 2002. Solar Physics 207, 323.
Forbes, T.G., 1991. Geophysical and Astrophysical Fluid Dynamics 63, 15.
Forbes, T.G., Priest, E.R., 1984. Solar Physics 94, 315.
Ishkov, V.N., 2001. Astronomical and Astrophysical Transactions 20, 563.
Kliem, B., Titov, V.S., Torok, T., 2004. Astronomy and Astrophysics 413, L23.
Lin, J., 2004. Solar Physics 219, 469.
Lin, R.P., Krucker, S., Hurford, G.J., et al., 2003. Astrophysical Journal 595, L69.
Mikic, Z., Barnes, D.C., Schnack, D.D., 1988. Astrophysical Journal 328, 830.
Podgorny, A.I., Podgorny, I.M., 1992. Solar Physics 139, 125.
Podgorny, A.I., Podgorny, I.M., 1998. Solar Physics 182, 159.
Podgorny, A.I., Podgorny, I.M., 2001. Astronomy Report 45, 60.
Podgorny, A.I., Podgorny, I.M., 2004. Computational Mathematics and Mathematical Physics 44, 1784.
Podgorny, A.I., Podgorny, I.M., 2006. Astronomy Report 50, 842.
Rickard, G.J., Priest, E.R., 1994. Solar Physics 151, 107.
Roussev, I.I., Sokolov, I.V., Forbes, T.G., Gombosi, M.A., Lee, M.A., Sakai, J.I., 2004. Astrophysical Journal 605, L73.
Tsuneta, S., Masuda, S., Kosugi, T., Sato, J., 1997. Astrophysical Journal 478, 787.